ACS APPLIED MATERIALS & INTERFACES

Research Article

www.acsami.org

Evaluation of Injectable Strontium-Containing Borate Bioactive Glass Cement with Enhanced Osteogenic Capacity in a Critical-Sized Rabbit Femoral Condyle Defect Model

Yadong Zhang,[†,⊥] Xu Cui,[‡,⊥] Shichang Zhao,[†,⊥] Hui Wang,[‡] Mohamed N. Rahaman,[*,§] Zhongtang Liu,[∥] Wenhai Huang,[‡] and Changqing Zhang[*,†]

[†]Department of Orthopedic Surgery, Shanghai Sixth People's Hospital, Shanghai Jiao Tong University, Shanghai 200233, People's Republic of China

[‡]School of Materials Science and Engineering, Tongji University, Shanghai 200092, People's Republic of China

[§]Department of Materials Science and Engineering, Missouri University of Science and Technology, Rolla, Missouri 65409, United States

[∥]Department of Orthopedics, Changhai Hospital, Second Military Medical University, Shanghai 200433, People's Republic of China

ABSTRACT: The development of a new generation of injectable bone cements that are bioactive and have enhanced osteogenic capacity for rapid osseointegration is receiving considerable interest. In this study, a novel injectable cement (designated Sr-BBG) composed of strontium-doped borate bioactive glass particles and a chitosan-based bonding phase was prepared and evaluated in vitro and in vivo. The bioactive glass provided the benefits of bioactivity, conversion to hydroxyapatite, and the ability to stimulate osteogenesis, while the chitosan provided a cohesive biocompatible and biodegradable bonding phase. The Sr-BBG cement showed the ability to set in situ (initial setting time = 11.6 ± 1.2 min) and a compressive strength of 19 ± 1 MPa. The Sr-BBG cement enhanced the proliferation and osteogenic differentiation of human bone marrow-derived mesenchymal stem cells in vitro when compared to a similar cement (BBG) composed of chitosan-bonded borate bioactive glass particles without Sr. Microcomputed tomography and histology of critical-sized rabbit femoral condyle defects implanted with the cements showed the osteogenic capacity of the Sr-BBG cement. New bone was observed at different distances from the Sr-BBG implants within eight weeks. The bone−implant contact index was significantly higher for the Sr-BBG implant than it was for the BBG implant. Together, the results indicate that this Sr-BBG cement is a promising implant for healing irregularly shaped bone defects using minimally invasive surgery.

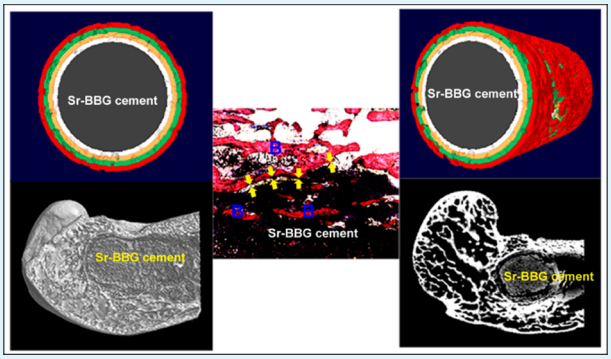

KEYWORDS: *injectable bone cement, borate bioactive glass, strontium-doped bioactive glass, osteoinductivity, rabbit femoral condyle defect model*

1. INTRODUCTION

Borate bioactive glasses have been receiving considerable research and development interest in recent years because of their attractive properties such as bioactivity, biocompatibility, and the ability to stimulate osteogenesis.[1−3] Because of their lower durability resulting from the borate glass network, borate bioactive glasses react faster and convert more completely to hydroxyapatite (HA) in an aqueous phosphate solution when compared to the silicate bioactive glasses such as 45S5 and 13−93.[4] To date, borate bioactive glasses have been studied and applied mainly in the form of porous scaffolds or granules. Three-dimensional (3D) porous scaffolds composed of borate bioactive glasses have shown the capacity to stimulate the proliferation and differentiation of osteogenic MLO-A5 cells and human bone marrow-derived mesenchymal stem cells (hBMSCs) in vitro and also to stimulate bone regeneration in rat calvarial defects in vivo.[2,3]

Implantation of 3D scaffolds and granules typically require open surgery. While granules are easier to handle during surgery, they can migrate into the surrounding tissue and are limited to the repair of nonloaded bone defects.[5] As 3D scaffolds cannot adequately fill bone defects, particularly defects with an irregular shape, they can lead to limited bone−implant contact (BIC) and poor osseointegration. Implantation of 3D scaffolds commonly requires machining of the graft to fit the defect shape prior to surgery or modifying the surgical site to match the implant shape. Those procedures can lead to a higher risk of surgery-related injuries, longer surgery time, and longer postoperative care.

Received: October 11, 2014
Accepted: January 15, 2015
Published: January 15, 2015

DOI: 10.1021/am507008z
ACS Appl. Mater. Interfaces 2015, 7, 2393−2403

Injecting a synthetic bone substitute directly into the defect site by minimally invasive surgery can potentially overcome some of the problems associated with 3D scaffolds and granules.[6,7] Consequently, there is considerable interest in the development of injectable cements for the repair of bone defects, in particular, large irregularly shaped defects. Bone cements for minimally invasive surgery should have the requisite injectability and setting time for ease of surgical implantation, bioactivity for bonding with bone, and the ability to serve as a carrier for local delivery of osteogenic or osteoinductive factors to facilitate cellular infiltration and subsequent integration with host bone.

Strontium (Sr), a trace element in the human body, has been reported to play a role in stimulating bone formation and inhibiting bone resorption.[8,9] The mechanism is believed to depend on the ability of Sr^{2+} ions to stimulate the alkaline phosphatase (ALP) activity and the osteogenic-related gene expression of mesenchymal stem cells (MSCs) and the expression of osteoprotegerin (OPG).[10−12] Sr has also been shown to enhance the proliferation and osteogenic differentiation of human osteoblast-like cells (MG-63) and BMSCs as well as the expression of angiogenic factors, which can lead to a coupling between angiogenesis and osteogenesis.[13−15] Systemic administration of strontium ranelate was found to increase bone mineral density (BMD), reduce the incidence of hip and vertebral fractures in osteoporotic patients,[16,17] and improve the peri-implant bone volume and implant pull-out strength in animals.[18,19] However, the bioavailability of strontium ranelate is low (<20% by oral administration), and the use of strontium ranelate has been associated with adverse effects such as cutaneous hypersensitivity, venous thrombosis, chronic renal failure, and osteomalacia.[20−22] Consequently, sustained local release of Sr^{2+} ions from implants could be preferable to systemic administration.

The release of Sr from different bone cements has been investigated recently. A Sr-containing poly(methyl methacrylate) (PMMA) bone cement was reported to show enhanced bioactivity and biocompatibility. Release of Sr^{2+} ions from the PMMA cement was believed to promote osteoblast proliferation and facilitate the precipitation of HA, leading to an increase in the strength of the bone−implant interface.[23,24] An injectable Sr-containing calcium phosphate cement (CPC) showed promising setting time, compressive strength, and radiopacity.[25] The cement stimulated the proliferation and differentiation of osteoblastic cells and hBMSCs in vitro[26,27] and enhanced new bone formation at the bone−cement interface and in the entire metaphyseal fracture defect area in rats.[28] However, PMMA cements commonly suffer from poor bonding with bone and high exothermic reaction in situ, while CPCs generally suffer from the need for high-temperature or elaborate processing techniques, slow degradation rate, and low strength.

The objective of the present study was to develop and evaluate an injectable bone cement composed of Sr-doped borate bioactive glass particles and a chitosan-based solution that served as the hardening phase. The Sr-doped bioactive glass was selected because of its bioactivity, osteogenic capacity, and the ability to release Sr^{2+} ions in a controlled manner. Chitosan is biocompatible and biodegradable,[29] and when dissolved in an aqueous medium, it produces a highly viscous solution. The characteristics of the cement, such as injectability, setting time, compressive strength, bioactivity, and degradation were evaluated. In vitro cell culture was used to assess the ability of the cement to stimulate the proliferation and osteogenic differentiation of hBMSCs. The capacity of the cement to stimulate bone formation at varying distances from the bone−cement interface was studied in a rabbit femoral condyle defect model using microcomputed tomography (micro-CT) and histology.

2. MATERIALS AND METHODS

2.1. Preparation of Sr-BBG Cement. The injectable cement developed in the present study (designated Sr-BBG) was formed from Sr-doped borate bioactive glass particles and a chitosan-based hardening solution. The Sr-doped bioactive glass was obtained by doping the parent bioactive glass (composition $6Na_2O$, $8K_2O$, 8MgO, 22CaO, $54B_2O_3$, $2P_2O_5$; mol %) with 9 mol % SrO. The glass was prepared by conventional melting and casting methods using the requisite amounts of analytical grade Na_2CO_3, K_2CO_3, $CaCO_3$, H_3BO_3, $(MgCO_3)_4{\cdot}Mg(OH){\cdot}25H_2O$, $NaH_2PO_4{\cdot}2H_2O$, and $SrCO_3$ and ground to form particles of size <40 μm. The hardening phase was prepared by mixing a chitosan solution (20 g of chitosan powder in 1 L of 1.0 M acetic acid) with a β-glycerophosphate solution (560 g of β-glycerophosphate in 1 L of deionized water) at a ratio of 7:1 by volume. (All chemicals were obtained from Sinopharm Chemical Reagent Co., Ltd., China). The Sr-BBG cement paste was prepared by manually mixing the glass particles with the hardening liquid at a powder-to-liquid ratio of 2.0 g/mL. For comparison, the cement (designated BBG) composed of the parent borate bioactive glass particles (without Sr) and the chitosan-based liquid was prepared by the same method. The cement paste was allowed to set in cylindrical polyethylene molds to form disc-shaped specimens for in vitro testing and cell culture experiments.

2.2. Injectability, Initial Setting Time, and Compressive Strength. The injectability of the cements was evaluated using an extrusion test described previously.[30] Briefly, after mixing, the paste was transferred into a commercial 10 mL syringe (diameter of opening = 1.7 mm). Then the paste was extruded from the syringe (held rigidly in a fixture) by applying a force of 100 N at a cross-head speed of 10 mm/min using a computer-controlled mechanical testing machine (CMT6104; SANS Test Machine Inc., China). The injectability coefficient (I) of the cements was defined as

$$I = [(M_o - M)/M_o] \times 100 \quad (1)$$

where M_o is the initial mass of the cement loaded into the syringe, and M is the mass remaining in the syringe after extrusion. Three samples of each cement were tested, and the results were expressed as a mean ± standard deviation (SD). The initial setting time of the cement pastes was measured using Gillmore needles according to ASTM C266−99. The compressive strength of cylindrical cement samples (5 mm in diameter ×10 mm) was measured using a CMY6104 SANS testing instrument at a cross-head speed of 0.5 mm min^{-1} and a preload of 1 kN. At least three samples of each cement were tested, and the mean strength ± SD was determined.

2.3. Evaluation of in Vitro Bioactivity and Degradation in Simulated Body Fluid. Simulated body fluid (SBF) with ion concentration nearly equal to that of human blood plasma was prepared according to the method described by Kokubo and Takadama.[31] The degradation of the cements was studied as a function of immersion time in SBF at 37 °C for as long as 90 d. Cylindrical samples of each cement (4.7 mm in diameter × 3.5 mm), preset for 4 h, were immersed in 10 mL of

DOI: 10.1021/am507008z
ACS Appl. Mater. Interfaces 2015, 7, 2393−2403

SBF in sterile polyethylene containers. At each time point, the samples were removed from the SBF, washed with deionized water, dried at 90 °C, and weighed. The SBF was cooled to room temperature, and its pH was measured using a pH meter (FE20; Mettler Toledo). At least three samples of each cement were measured at each immersion time, and the results were expressed as a mean ± SD.

The surface morphology and microstructure of the cement samples before and after immersion in SBF were examined in a field-emission scanning electron microscope (FESEM) fitted with an energy-dispersive X-ray (EDS) spectrometer (Hitachi S-4700; Tokyo, Japan). X-ray diffraction (XRD) (D/max-2500 V B2+/PC; Rig-aku, Tokyo, Japan) was used to determine the presence of crystalline phases in the cements before and after immersion in SBF. At each time point, the concentration of $(BO_3)^{3-}$ and Sr^{2+} ions in the SBF was measured using inductively coupled plasma atomic emission spectroscopy (ICP-AES; Optima 2100 DV; U.S.A.).

2.4. In Vitro Cell Culture. Primary hBMSCs were isolated and subcultured as previously described.[32] The use of the hBMSCs was approved by the Ethical Committee of Shanghai Sixth People's Hospital, Shanghai Jiao Tong University School of Medicine. Cells at the fourth to seventh passage were used for subsequent cell culture experiments.

2.4.1. Cell Adhesion and Proliferation. Cell adhesion and cell−biomaterial interaction were assessed by seeding 1×10^5 hBMSCs on BBG and Sr-BBG cement discs (6 mm in diameter × 3 mm) in 24-well culture plates. The cells were incubated in Dulbecco's modified Eagle's medium (DMEM; GIBCO, Invitrogen Pty Ltd., Australia) supplemented with 10% fetal calf serum (FCS; InVitro Technology, Australia). The cell cultures were maintained at 37 °C in a humidified atmosphere of 5% CO_2. After 3 d, the samples were removed from the culture wells, rinsed with phosphate-buffered saline (PBS), and fixed with 2.5% glutaraldehyde in PBS for 1 h. After removing the fixative by washing with a buffer containing 4% (w/v) sucrose in PBS, the samples were postfixed in 1% osmium tetroxide in PBS and dehydrated in a graded series of ethanol (50%, 70%, 90%, 95%, 100%) and hexamethyldisilazane (HMDS). The specimens were coated with gold and examined in an FESEM (Hitachi; S-4700).

A Cell Counting Kit-8 assay (CCK-8, Dojindo Molecular Technologies, Inc. Japan) was used to assess the proliferation of hBMSCs on the BBG and Sr-BBG cement discs. Briefly, 1×10^4 hBMSCs were seeded on each cement disc and cultured for 1, 3, and 7 d. Then 360 μL of culture medium and 40 μL of the CCK-8 solution were added to each well at each time point, and the system was incubated at 37 °C for another 4 h. An aliquot of 100 μL was taken from each well and transferred to a fresh 96-well plate. The absorbance of these samples was measured at 450 nm using a spectrophotometric microplate reader (Bio-Rad 680, U.S.A.). The results were determined as the optical density minus the absorbance of the blank wells.

2.4.2. Cell Differentiation. ALP activity was measured after seeding 1×10^5 hBMSCs on discs of each cement and culturing for 7 and 14 d. The experiments were performed in triplicate. At each time point, the culture medium was decanted, and the cell layer was washed gently three times with PBS and then once in cold 50 mM Tris buffer. Then the hBMSCs were lysed in 200 μL of 0.2% Triton X-100. Lysates were sonicated after being centrifuged at 14 000 rpm for 15 min at 4 °C. Supernatant (50 μL) was mixed with 150 μL of working solution according to the manufacturer's protocol (Beyotime Biotech, China). The conversion of *p*-nitrophenylphosphate into *p*-nitrophenol in the presence of ALP was determined by measuring the absorbance at 405 nm using a microplate reader (Bio-Rad 680, U.S.A.). All samples were assayed in triplicate. The ALP activity was calculated from a standard curve after normalizing to the total protein content, and the results were expressed in mM of *p*-nitrophenol produced per minute per milligram of protein.

The expression levels of the osteogenic-related genes, runt-related transcription factor 2 (RUNX2), osteocalcin (OCN), bone morphogenetic protein-2 (BMP-2), type I collagen (COL-1), and bone sialoprotein (BSP) were measured using qRT-PCR. The cells were seeded at a density of 2×10^4 cells/disc, cultured for 7 and 14 d, and then harvested using TRIzol reagent (Invitrogen Pty Ltd., Australia) to extract the RNA. Then the RNA was reverse-transcribed into complementary DNA (cDNA) using a Revert Aid First Strand cDNA Synthesis Kit (Thermo Scientific). The qRT-PCR analysis was performed on an ABI Prism 7300 Thermal Cycler (Applied Biosystems, Australia) using SYBR Green detection reagent. The relative expression of the genes was normalized against the housekeeping gene GAPDH. All samples were assayed in triplicate. The relative expression was calculated using the formula $2^{-(\text{normalized average Ct})} \times 100$.

2.5. In Vivo Evaluation of Sr-BBG Cement in a Rabbit Femoral Condyle Defect Model. *2.5.1. Surgical Procedure and Treatment.* All animal experimental procedures were approved by the Animal Research Committee of Shanghai Sixth People's Hospital, Shanghai Jiao Tong University School of Medicine. A total of 12 adolescent male New Zealand white rabbits weighing 3.0−3.5 kg were used. The rabbits were anesthetized using an intramuscular injection of 50 mg/kg ketamine hydrochloride and 5 mg/kg xylazine. Lateral approach was performed to expose the distal femoral epiphysis, and a critical-sized condyle defect (6 mm diameter and 12 mm depth) was created with an electric trephine (Nouvag AG, Goldach, Switzerland) under irrigation with 0.9% sterile saline solution. Mixing of the cement components started after the femoral defect was surgically created. Then the BBG or Sr-BBG cement paste was injected into the defects using a syringe (six defects filled with Sr-BBG and six with BBG), and the wounds were sutured. Prophylactic antibiotic was given for 3 d.

2.5.2. Microcomputed Tomography. The animals were euthanized under general anesthesia at four or eight weeks postimplantation, and the femoral condyles were explanted and fixed in 4% paraformaldehyde. The morphology of the reconstructed femurs was assessed using micro-CT (Skyscan 1176, Kontich, Belgium). Scanning was performed at a resolution of 18 μm. Images were reconstructed based on the Feldkamp convolution back-projection algorithm and segmented into binary images using adaptive local thresholding. The percentage of new bone volume relative to tissue volume (BV/TV) and the trabecular bone pattern factor (Tb.Pf) were calculated at different distances from the cement implant surface (at 6, 12, 18, and 24 pixels; 1 pixel ≈ 18 μm).

2.5.3. Histologic Processing. After dehydration in a graded series of ethanol (75−100%), the undecalcified specimens were embedded in PMMA. Transverse sections were cut, ground, and polished to a final thickness of ∼40 μm.[33] The sections were stained with Van Gieson's picrofuchsin to identify new bone formation at the bone−cement interface. The bone and cement were stained red and black, respectively. The contact percentage giving the extent to which the mineralized bone was

DOI: 10.1021/am507008z
ACS Appl. Mater. Interfaces 2015, 7, 2393−2403

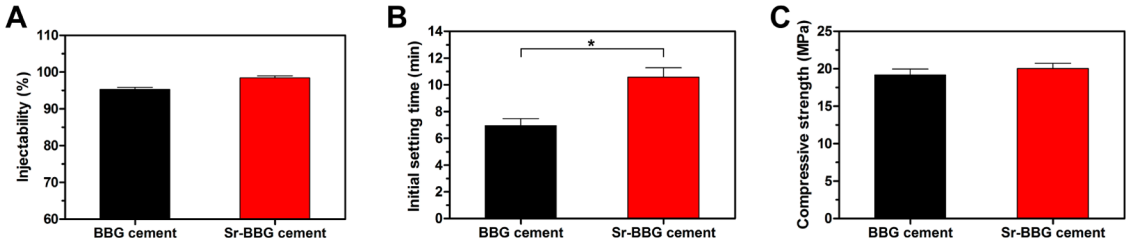

Figure 1. Physical properties of BBG and Sr-BBG cements. (A) Injectability (determined from eq 1). (B) Initial setting time. (C) Compressive strength. *Significant difference between groups ($p < 0.05$).

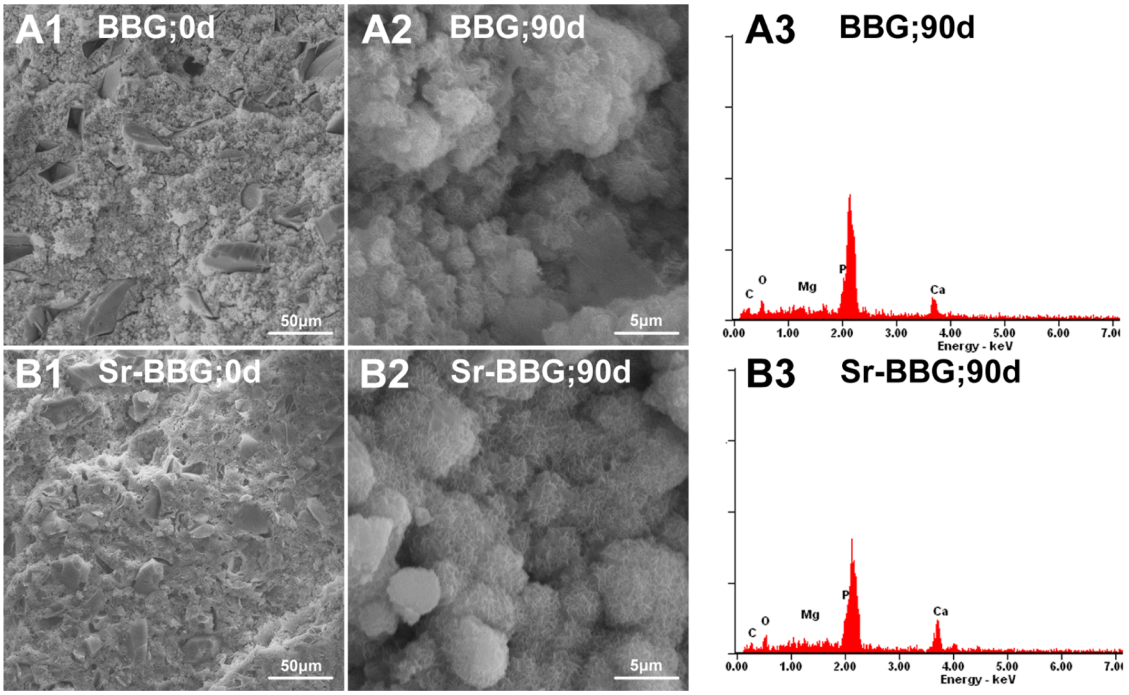

Figure 2. SEM images and EDS analysis of BBG and Sr-BBG cements before (0 d) and after immersion in SBF for 90 d. SEM images of the surface of BBG and Sr-BBG cement as fabricated (after hardening) (A1 and B1) and after immersion for 90 d (A2 and B2). EDS spectra of the surface of the BBG and Sr-BBG cements after immersion for 90 d (A3 and B3).

attached directly to the cement (i.e., the BIC index) was measured.

2.6. Statistical Analysis. The data were expressed as a mean ± SD. An independent Student's t test was used to compare differences between groups, and a p value of <0.05 was considered to be statistically significant.

3. RESULTS

3.1. Characteristics of Sr-BBG Cement. The injectability, initial setting time, and compressive strength of the BBG and Sr-BBG cements are shown in Figure 1. The injectability of the Sr-BBG cement (98 ± 1%) was not significantly different from that of the BBG cement (95 ± 1%) (Figure 1A). There was no phase separation of the cements on extrusion from the syringe, which might be attributed to the cohesiveness between the bioactive glass particles and the chitosan hardening solution.[34] The initial setting time of the Sr-BBG cement (10.6 ± 1.2 min) was significantly longer than that for the BBG cement (7.3 ± 0.9 min), (Figure 1B), indicating a retarding effect of Sr on the setting of the cement. There was no significant difference between the compressive strength of the hardened Sr-BBG and BBG cements (19 ± 1 MPa and 20 ± 1 MPa, respectively) (Figure 1C).

Figure 2 shows scanning electron microscopy (SEM) images and EDS spectra of the surface of the BBG and Sr-BBG cements before and after immersion in SBF. The as-prepared cements showed a rough surface in which some glass particles and large pores were visible (Figure 2A1,B1). Upon immersion in SBF, a product was formed on the surface of the cements within 20 d. At 90 d, the surface was composed of nearly globular particles (Figure 2A2,B2). EDS analysis of the surface of the cements immersed for 90 d in SBF showed major peaks corresponding to Ca and P, indicating the formation of a calcium phosphate material (Figure 2A3,B3). The Ca/P atomic ratio of the material formed on the BBG and Sr-BBG cement was 1.54 and 1.62, respectively.

XRD showed that the as-prepared Sr-BBG cement was amorphous (Figure 3). After immersion for 20 d in SBF, the XRD pattern showed a broad peak of low intensity (height) that corresponded to the main peak in a reference HA (JCPDS 72−1243). The broad low-intensity peak might be an indication that the as-formed HA had not fully crystallized, that the crystallite size of the HA product was in the nanometer range, or a combination of both. The peak intensity increased, and a second HA peak appeared, as the immersion time was

DOI: 10.1021/am507008z
ACS Appl. Mater. Interfaces 2015, 7, 2393−2403

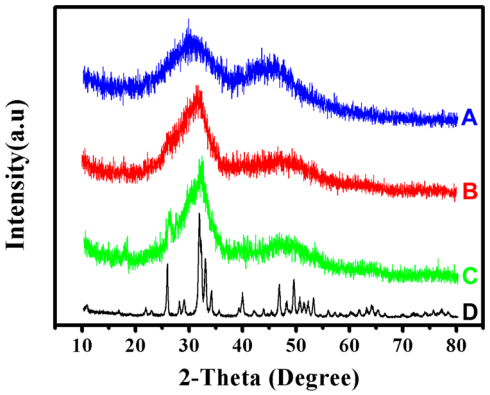

Figure 3. XRD patterns of Sr-BBG cement before (A) and after immersion in SBF for 20 d (B) and 90 d (C). The pattern of a reference hydroxyapatite (JCPDS 72−1243) (D) is shown for comparison.

increased to 90 d. The XRD patterns for the BBG cement were similar to those in Figure 3, and they are omitted for brevity.

Figure 4 shows the weight loss of the cements, the pH value of the SBF, and the amount of borate $(BO_3)^{3-}$ and Sr^{2+} ions released from the cements as a function of immersion time in SBF. The weight loss increased rapidly in the first 5−10 d but slowed considerably thereafter (Figure 4A). At any given immersion time, the weight loss of the Sr-BBG cement was smaller than that of the BBG cement. The pH of the SBF also increased rapidly during the first 5−10 d, but it decreased gradually at longer immersion times (Figure 4B). The pH of the SBF reacted with the Sr-BBG cement was smaller than that for the BBG cement at immersion times less than ~60 d, but there was no significant difference in the pH when the experiments were terminated at 90 d. There was little difference in the amount of $(BO_3)^{3-}$ ions released from the BBG and Sr-BBG cements into the SBF (Figure 4C). The amount of Sr^{2+} ions released from the Sr-BBG cement into the SBF increased with immersion time, reached a maximum at approximately day 20 and decreased slowly thereafter (Figure 4D).

3.2. Adhesion and Proliferation of hBMSCs on Sr-BBG Cement. SEM images of the cements after 3 d of culture showed that the presence of hBMSCs with a well-spread morphology on the surface of both cements (Figure 5). The number of hBMSCs per unit area of the Sr-BBG cement surface was higher than that for BBG cement. The CCK-8 proliferation assay showed that both cements supported the proliferation of hBMSCs (Figure 6). The number of cells increased with culture time (1, 3, and 7 d) and, at days 3 and 7, the number of cells on the Sr-BBG cement was significantly higher than it was on the BBG cement ($p < 0.05$), which is consistent with the SEM observation.

3.3. Differentiation of hBMSCs on Sr-BBG Cement. At both culture times (7 and 14 d), the ALP activity and osteogenic gene expression (RUNX2, OCN, BMP-2, COL-1, and BSP) of the hBMSCs cultured on the Sr-BBG cement were significantly higher when compared to those of the hBMSCs cultured on the BBG cement (Figures 7 and 8). The results showed that the Sr-BBG cement had a significantly better ability to stimulate osteogenic differentiation of hBMSCs at both time points when compared to the BBG cement.

3.4. Bone Regeneration and Integration of Sr-BBG Cement in Vivo. *3.4.1. Microcomputed Tomography Analysis.* Micro-CT imaging of the rabbit femoral condyle defects implanted with the Sr-BBG cement showed a small amount of newly formed bone surrounding the implant at four weeks postimplantation and more extensive bone formation at the bone−cement interface at eight weeks. In comparison, it appeared that a smaller amount of new bone was formed at the periphery of the BBG cement at four weeks. However, a difference in the amount of newly formed bone at the periphery of the BBG and Sr-BBG cements could not be clearly observed from the micro-CT images at eight weeks (Figure 9). The volume of new bone formed at varying distances from the

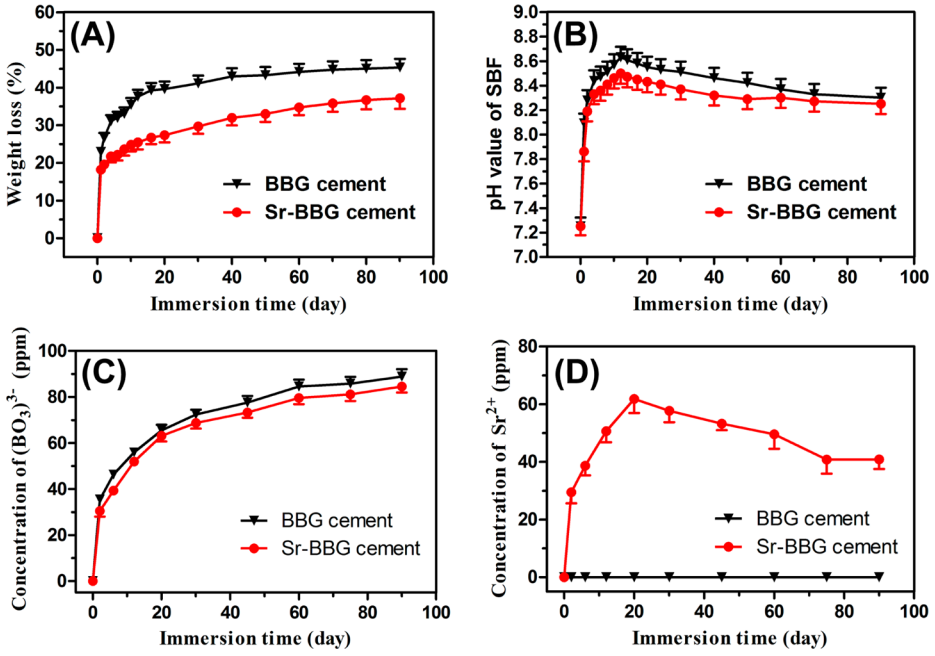

Figure 4. Weight loss of the BBG and Sr-BBG cements (A), pH of the medium (B), and concentration of $(BO_3)^{3-}$ ions (C) and Sr^{2+} ions (D) in the medium as a function of immersion time of the cements in SBF.

DOI: 10.1021/am507008z
ACS Appl. Mater. Interfaces 2015, 7, 2393−2403

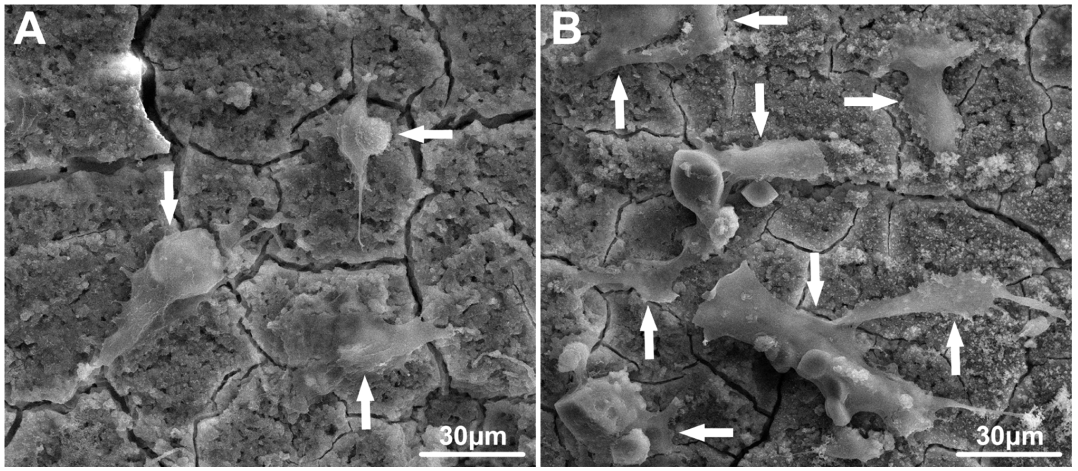

Figure 5. SEM images showing the attachment of hBMSCs on BBG (A) and Sr-BBG (B) cement after culturing for 3 d.

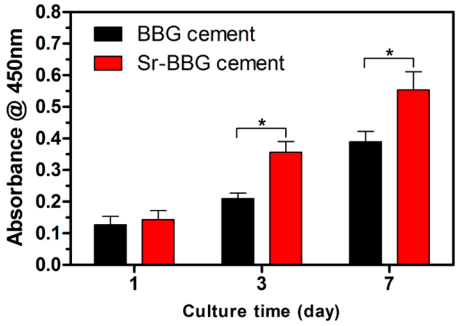

Figure 6. Proliferation of hBMSCs cultured on BBG and Sr-BBG cements for 1, 3, and 7 d. *Significant difference between groups ($p < 0.05$).

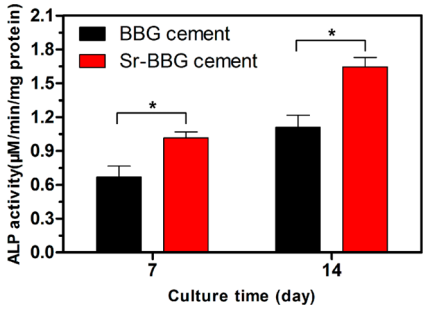

Figure 7. ALP activity of hBMSCs cultured on BBG and Sr-BBG cements for 7 and 14 d. *Significant difference between groups ($p < 0.05$).

bone−cement interface was determined to quantitatively assess the osteogenic capacity of the cements. As shown in Table 1, the BV/TV at varying distances from the periphery of the Sr-BBG cement was significantly higher than that for the BBG cement at both four and eight weeks postimplantation. In addition, the Tb.Pf (an index that decreases with increase in bone mass) at varying distances from the periphery of the Sr-BBG implants was significantly lower than that for the BBG implants at four and eight weeks postimplantation. The results indicated that the Sr-BBG cement had a better capacity to stimulate bone regeneration at the interfacial areas when compared to the BBG cement for the implantation periods used.

3.4.2. Histomorphometric Analysis. The bone−cement contact was further assessed using histomorphometric analysis at four and eight weeks postimplantation (Figure 10A). Van Gieson's picrofuchsin stained sections showed that both cements were well-tolerated in the defect sites and that there were no signs of rejection, necrosis or infection. At four weeks postimplantation, there was only a small amount of newly formed bone, and large gaps were evident around the BBG cement. In comparison, for the Sr-BBG cement, the amount of newly formed bone appeared to higher, and the gaps around the cement were noticeably smaller. With an increase in the implantation time to eight weeks, small gaps infiltrated with fibrous tissue were still present around the BBG cement, suggesting limited bone−cement contact. In comparison, no infiltration of fibrous tissue between the bone and the implant was observed for the Sr-BBG cement, indicating direct bone−cement contact. Bone ingrowth into the voids formed as a result of the degradation of the Sr-BBG cement was observed at eight weeks postimplantation, showing superior osseointegration when compared to the BBG cement. The BIC index for the Sr-BBG cement implant was 26 ± 6% and 36 ± 9%, respectively, at four and eight weeks postimplantation, which was significantly higher than these same values for BBG cement implant, 13 ± 3% (four weeks) and 26 ± 4% (eight weeks) (Figure 10B).

4. DISCUSSION

An injectable cement (Sr-BBG) composed of Sr-doped borate bioactive glass particles and a chitosan-based bonding phase was developed and evaluated in vitro and in vivo. In addition to being bioactive and biodegradable, the cement showed clinically relevant injectability and setting time and the ability to stimulate not only the osteogenic differentiation of hBMSCs in vitro but also bone regeneration and integration in vivo.

The setting time is an important property for a cement that is intended for clinical applications. Hardening of the cement should occur neither too quickly (to allow time for molding and injection) nor too slowly (to prevent migration to undesirable sites and the need to close the defect site immediately after injection).[35] The Sr-BBG cement in the present study showed a setting time of 10.6 ± 1.2 min that was in the suggested clinical range of 10−15 min.[36] The Sr-BBG cement also showed excellent injectability (98 ± 1%) at room temperature. Together, these properties indicate that the Sr-

DOI: 10.1021/am507008z
ACS Appl. Mater. Interfaces 2015, 7, 2393−2403

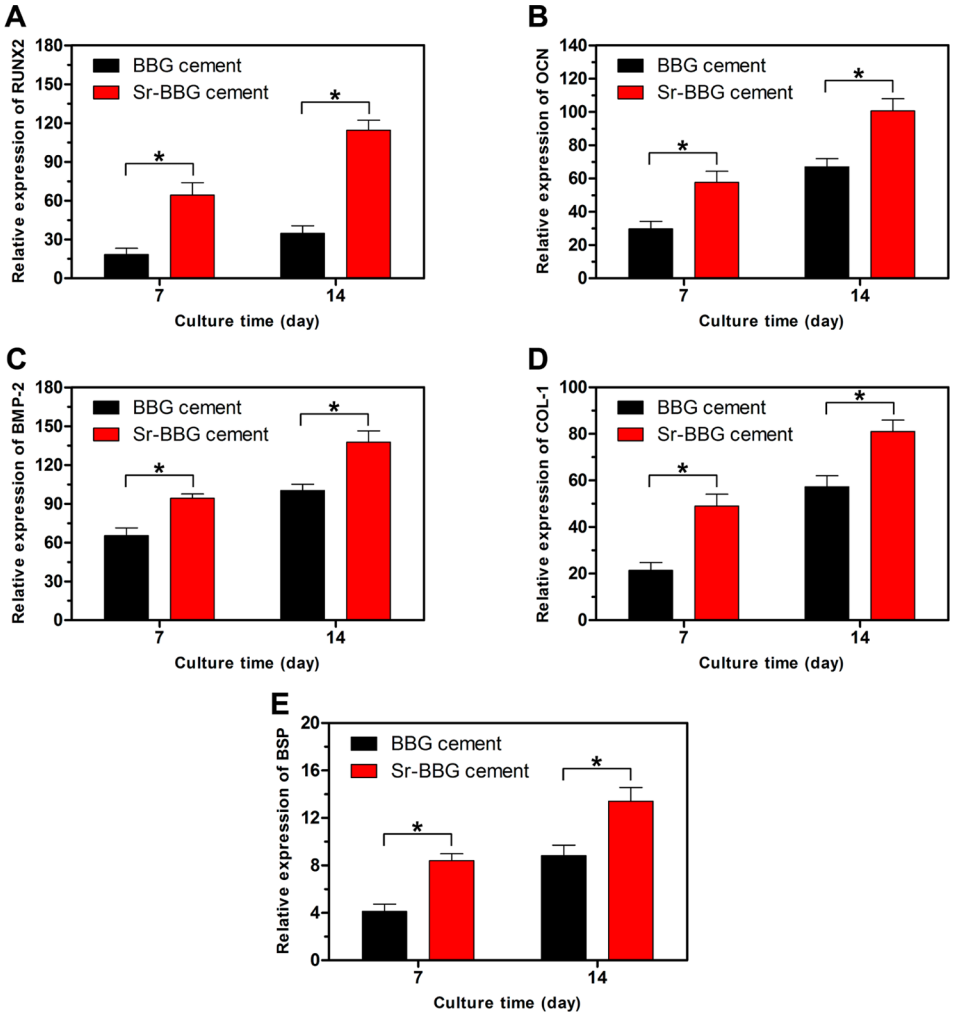

Figure 8. Osteogenic gene expression of RUNX2 (A), OCN (B), BMP-2 (C), COL-1 (D), and BSP (E) for hBMSCs cultured on BBG and Sr-BBG cement discs as determined by qRT-PCR analysis after 7 and 14 d. *Significant difference between groups ($p < 0.05$).

BBG cement might have promising potential for implantation by minimally invasive surgery.

The strength of the hardened cement is another important property in bone-repair applications.[37] The compressive strength of the Sr-BBG cement (19 ± 1 MPa) was almost twice the highest compressive strength of human trabecular bone, indicating that the cement could be used for regenerating bone in some load-bearing sites. The high strength of the cement is believed to be a direct result of the chitosan hardening phase that undergoes a sol−gel transition, forming a strong cohesive bonding phase.

The formation of HA on the surface of a biomaterial plays an important role in enhancing its bonding to bone.[38] XRD patterns of the Sr-BBG and BBG cements showed a major peak corresponding to HA within 20 d of immersion in SBF. The intensity of the peak increased, and a second HA peak appeared as the immersion time was increased to 90 d. Formation of an HA layer on the Sr-BBG cement immersed in SBF for 90 d was also confirmed by SEM and EDS analyses.

The interaction of a biomaterial with cells is a key factor in osseointegration. Cell adhesion is the initial step of cellular interaction with the surface of an implant. It is a key regulator of cell proliferation, differentiation, activation, and migration, which can determine the fate of the biological interaction at the interface with the implant. SEM images and assays of cell proliferation showed a significantly larger number of cells on the Sr-BBG cement at incubation times of 3 and 7 d when compared to the BBG cement. These trends are compatible with the results of a previous study, which showed a better ability of Sr-doped HA to support the attachment and proliferation of human osteoprecursor cells when compared to undoped HA.[39]

The composition of a biomaterial could affect the biological response of cells due to dissolution of ions from biomaterial.[40,41] The effect of Sr^{2+} ions on the proliferation and osteogenic differentiation of osteoblasts or MSCs has been investigated previously. One study found a maximum in osteogenic marker expression at Sr^{2+} concentrations of 5×10^{-2} mM but an inhibitory effect on the proliferation of primary human osteoblasts at Sr^{2+} concentrations greater than 1 mM.[42] Other studies showed a stimulating effect on ALP expression and bone nodule formation in MSC cultures at Sr^{2+} concentrations of up to 2 mM and a positive influence on long-term cultures of MC3T3-E1 cells at Sr^{2+} concentrations of up to 1 mM.[43,44] The upper limit of the Sr^{2+} concentration released by Sr-BBG cement in the present study (~70 ppm or 7×10^{-2} mM) was in the range reported to stimulate proliferation and osteogenic differentiation of cells of the osteoblastic lineage.[43]

DOI: 10.1021/am507008z
ACS Appl. Mater. Interfaces 2015, 7, 2393−2403

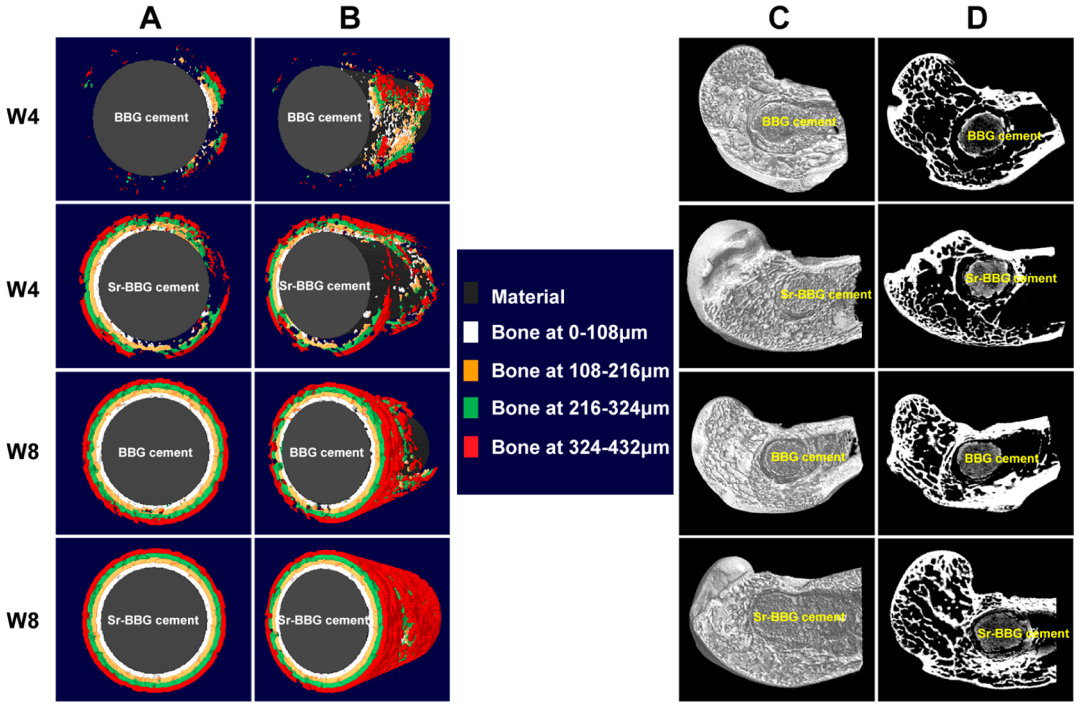

Figure 9. 3D reconstructed images (columns A, B, and C) and sagittal images (column D) by micro-CT imaging of the area surrounding the cement implants, showing newly formed bone at different distances from the edge of the cement after implantation for four weeks (W4) and eight weeks (W8) in critical-sized rabbit femoral condyle defects.

Table 1. Bone Structural Parameters at Different Distances from the Surface of the Sr-BBG and BBG Cements Implanted for Four and Eight Weeks in Critical-Sized Rabbit Femoral Condyle Defects

sample		BBG cement		Sr-BBG cement	
time (w)	distance (μm)	BV/TV[a] (%)	Tb.Pf[a] (mm^{-1})	BV/TV[a] (%)	Tb.Pf[a] (mm^{-1})
4	216	6	23	26	9
4	432	10	19	33	6
8	216	30	10	42	4
8	432	42	6	56	2

[a]BV/TV: bone volume/total volume; Tb.Pf: bone trabecular pattern factor. Data correspond to a representative rabbit in each experimental group.

The results of the present study showed that the Sr-BBG cement significantly enhanced the expression of osteogenic genes (RUNX2, OCN, BMP-2, COL-1, and BSP) at both incubation times used (7 and 14 d). Type I collagen (COL-1) is an early marker for cell maturation, whereas OCN is a terminal marker gene for osteogenic differentiation. Thus, the Sr-BBG cement appeared to support both the cell maturation and early terminal osteoblast differentiation. These results are compatible with those of previous studies.[43,45,46] Strontium-doped HA materials have been shown to promote the proliferation, osteogenic differentiation, and vascular endothelial growth factor (VEGF) expression of human osteoblast-like cells (MG-63).[13] One of the potential mechanisms for osteogenesis is enhanced angiogenesis. Activation of VEGF receptors can induce the expression of genes associated with osteogenesis and angiogenesis, such as RUNX2, BMP-2, and

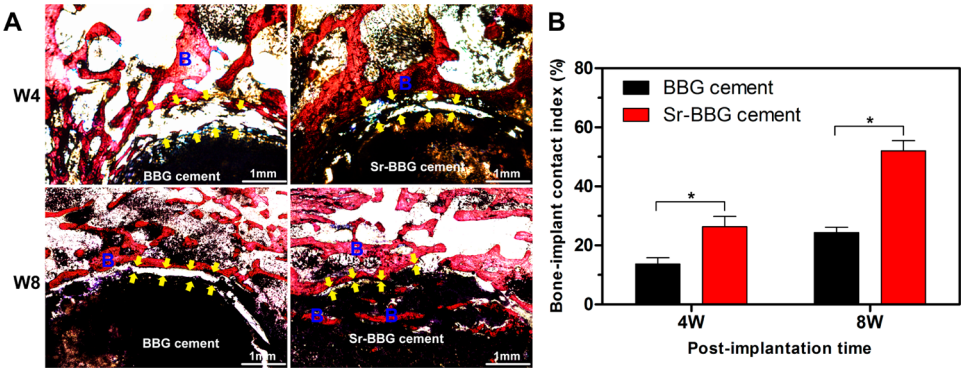

Figure 10. Histological analysis of newly formed bone and bone−implant contact (BIC) index for BBG and Sr-BBG cements implanted for four and eight weeks in critical-sized rabbit femoral condyle defects. (A) Undecalcified sections stained with Van Gieson's picrofuchsin. The new bone appears red, and the cement appears black. B indicates bone; yellow arrows indicate BIC area. (B) BIC index for the BBG and Sr-BBG cements determined from the histomorphometric measurements.

DOI: 10.1021/am507008z
ACS Appl. Mater. Interfaces 2015, 7, 2393−2403

osteopontin (OPN). RUNX2, BMP-2, and OPN are sequentially expressed during osteogenesis. As a result of a positive feedback mechanism, a higher expression of RUNX2, BMP-2, and OPN could further promote the secretion of VEGF, which, in turn, could stimulate an angiogenic response.

The substitution of Sr for Ca in mesoporous bioactive glass (MBG) scaffolds was found to modify the dissolution of Ca^{2+} and Si^{4+} ions from the MBG and to better stabilize the pH around the scaffolds when compared to MBG scaffolds without Sr.[45] The ions released from the Sr-BBG cement and the more stable pH environment due to its degradation could stimulate the metabolic activity, proliferation, and differentiation of the MSCs (BMP-2 expression).[40,41,47]

Strontium can also affect cellular activity via the membrane-bound calcium sensing receptor (CaSR) in both osteoblasts and osteoclasts.[48−50] Since Sr^{2+} ions have shown a positive influence on the Wnt/β-catenin pathway by triggering mitogenic signaling,[51] it is possible that the presence of Sr^{2+} ions could enhance the ability of MSCs and preosteoblasts to proliferate and differentiate into bone-forming osteoblasts and promote the formation of extracellular matrix.[43,44,48] In the present study, the Sr^{2+} ions released from the Sr-BBG cement presumably created a better microenvironment for osteogenesis, resulting in enhanced adhesion, proliferation, and differentiation of the hBMSCs.

Implantation of the Sr-BBG cement in critical-sized rabbit femoral condyle defects provided a method for evaluating its potential in eventual clinical application. The Sr-BBG cement significantly enhanced osteogenesis at the interfacial areas, stimulated greater bone formation, and showed a higher BIC index when compared to the BBG cement. Bone ingrowth into the Sr-BBG cement occurred within eight weeks of implantation, indicating better osseointegration when compared to the BBG cement. The better osseointegration could have a positive effect in improving the fixation of implants while concurrently reducing the activation of osteoclasts and preventing long-term host bone resorption and implant failure.

Our in vivo results are compatible with those of previous studies that showed better bone formation and BIC of Sr-substituted HA coatings[52] and Sr-doped HA bone-graft extender.[53] Local delivery of Sr^{2+} from surface-functionalized titanium implants was found to enhance BIC in the femoral shaft of rats.[22] It has been suggested that bone ingrowth into bone cements could decrease bone resorption and promote the formation of a stable interface.[54] Previous studies attributed the enhanced new bone formation by Sr^{2+} ions to the increased osteogenic differentiation of endogenous MSCs.[43,55]

While an in-depth study of the molecular mechanisms was beyond the scope of the present study, the results indicated that several factors might be responsible for the better ability of the Sr-BBG cement to improve bone regeneration and BIC when compared to the BBG cement. Those factors include the ability of the cement to mineralize to HA, provide a sustained delivery of Sr^{2+} ions in the defect site, and enhance the secretion of angiogenic factors. The release of Sr^{2+} ions could also modify the alkaline microenvironment produced by the degradation of BBG cements, resulting in a more stable pH environment that could further stimulate the metabolic activity, proliferation, and differentiation of mesenchymal progenitor cells.

5. CONCLUSIONS

A novel injectable cement (designated Sr-BBG) developed in the present study, composed of Sr-doped borate bioactive glass particles and a chitosan-based hardening phase, showed clinically relevant injectability and setting time, as well as bioactivity due to the bioactive glass phase. When compared to a similar cement (designated BBG) composed of the borate glass particles without Sr, the Sr-BBG cement enhanced the proliferation and osteogenic differentiation of hBMSCs in vitro. The Sr-BBG cement showed a better capacity than the BBG cement to regenerate bone at the implant−bone interface at four and eight weeks postimplantation in a critical-sized rabbit femoral condyle defect model. By combining its osteogenic capacity with the ability to serve as a carrier for pharmaceuticals or growth factors, the Sr-BBG cement could provide an attractive implant to treat irregularly shaped bone defects using minimally invasive surgery.

AUTHOR INFORMATION

Corresponding Authors

*Phone: +1 573-341-4406. E-mail: rahaman@mst.edu. (M.N.R.)

*Phone: +86 21 64369181. E-mail: shzhangchangqing@163.com. (C.-Q.Z.)

Author Contributions

⊥These authors contributed equally to this work.

Notes

The authors declare no competing financial interest.

ACKNOWLEDGMENTS

The authors acknowledge the support of the National Natural Science Foundation of China (Nos. 51372170, 81371936, and 81371938) and the Science and Technology Commission of Shanghai Municipality (No. 12JC1408500).

REFERENCES

(1) Zhang, X.; Jia, W.; Gu, Y.; Xiao, W.; Liu, X.; Wang, D.; Zhang, C.; Huang, W.; Rahaman, M. N.; Day, D. E.; Zhou, N. Teicoplanin-Loaded Borate Bioactive Glass Implants for Treating Chronic Bone Infection in a Rabbit Tibia Osteomyelitis Model. *Biomaterials* **2010**, *31*, 5865−5874.

(2) Bi, L.; Rahaman, M. N.; Day, D. E.; Brown, Z.; Samujh, C.; Liu, X.; Mohammadkhah, A.; Dusevich, V.; Eick, J. D.; Bonewald, L. F. Effect of Bioactive Borate Glass Microstructure on Bone Regeneration, Angiogenesis, and Hydroxyapatite Conversion in a Rat Calvarial Defect Model. *Acta Biomater.* **2013**, *9*, 8015−8026.

(3) Gu, Y.; Huang, W.; Rahaman, M. N.; Day, D. E. Bone Regeneration in Rat Calvarial Defects Implanted with Fibrous Scaffolds Composed of a Mixture of Silicate and Borate Bioactive Glasses. *Acta Biomater.* **2013**, *9*, 9126−9136.

(4) Brown, R. F.; Rahaman, M. N.; Dwilewicz, A. B.; Huang, W.; Day, D. E.; Li, Y.; Bal, B. S. Effect of Borate Glass Composition on Its Conversion to Hydroxyapatite and on the Proliferation of Mc3t3-E1 Cells. *J. Biomed. Mater. Res., Part A* **2009**, *88*, 392−400.

(5) Hotz, G. Alveolar Ridge Augmentation with Hydroxylapatite Using Fibrin Sealant for Fixation: Part Ii: Clinical Application. *Int. J. Oral Maxillofac. Surg.* **1991**, *20*, 208−213.

(6) Kretlow, J. D.; Young, S.; Klouda, L.; Wong, M.; Mikos, A. G. Injectable Biomaterials for Regenerating Complex Craniofacial Tissues. *Adv. Mater.* **2009**, *21*, 3368−3393.

(7) Xu, H. H.; Weir, M. D.; Simon, C. G. Injectable and Strong Nano-Apatite Scaffolds for Cell/Growth Factor Delivery and Bone Regeneration. *Dent. Mater.* **2008**, *24*, 1212−1222.

(8) Reginster, J. Y. Strontium Ranelate in Osteoporosis. *Curr. Pharm. Des.* **2002**, *8*, 1907−1916.

(9) Buehler, J.; Chappuis, P.; Saffar, J.; Tsouderos, Y.; Vignery, A. Strontium Ranelate Inhibits Bone Resorption While Maintaining Bone

DOI: 10.1021/am507008z
ACS Appl. Mater. Interfaces 2015, 7, 2393−2403

Formation in Alveolar Bone in Monkeys (Macaca Fascicularis). *Bone* **2001**, *29*, 176−179.
(10) Peng, S.; Zhou, G.; Luk, K. D.; Cheung, K. M.; Li, Z.; Lam, W. M.; Zhou, Z.; Lu, W. W. Strontium Promotes Osteogenic Differentiation of Mesenchymal Stem Cells through the Ras/Mapk Signaling Pathway. *Cell. Physiol. Biochem.* **2009**, *23*, 165−174.
(11) Marie, P.; Felsenberg, D.; Brandi, M. How Strontium Ranelate, Via Opposite Effects on Bone Resorption and Formation, Prevents Osteoporosis. *Osteoporosis Int.* **2011**, *22*, 1659−1667.
(12) Saidak, Z.; Marie, P. J. Strontium Signaling: Molecular Mechanisms and Therapeutic Implications in Osteoporosis. *Pharmacol. Ther.* **2012**, *136*, 216−226.
(13) Lin, K.; Liu, P.; Wei, L.; Zou, Z.; Zhang, W.; Qian, Y.; Shen, Y.; Chang, J. Strontium Substituted Hydroxyapatite Porous Microspheres: Surfactant-Free Hydrothermal Synthesis, Enhanced Biological Response and Sustained Drug Release. *Chem. Eng. J.* **2013**, *222*, 49−59.
(14) Lin, K.; Xia, L.; Li, H.; Jiang, X.; Pan, H.; Xu, Y.; Lu, W. W.; Zhang, Z.; Chang, J. Enhanced Osteoporotic Bone Regeneration by Strontium-Substituted Calcium Silicate Bioactive Ceramics. *Biomaterials* **2013**, *34*, 10028−10042.
(15) Bose, S.; Fielding, G.; Tarafder, S.; Bandyopadhyay, A. Understanding of Dopant-Induced Osteogenesis and Angiogenesis in Calcium Phosphate Ceramics. *Trends Biotechnol.* **2013**, *31*, 594−605.
(16) Meunier, P. J.; Roux, C.; Seeman, E.; Ortolani, S.; Badurski, J. E.; Spector, T. D.; Cannata, J.; Balogh, A.; Lemmel, E. M.; Pors-Nielsen, S.; Rizzoli, R.; Genant, H. K.; Reginster, J. Y. The Effects of Strontium Ranelate on the Risk of Vertebral Fracture in Women with Postmenopausal Osteoporosis. *N. Engl. J. Med.* **2004**, *350*, 459−468.
(17) Reginster, J. Y.; Felsenberg, D.; Boonen, S.; Diez-Perez, A.; Rizzoli, R.; Brandi, M. L.; Spector, T. D.; Brixen, K.; Goemaere, S.; Cormier, C.; Balogh, A.; Delmas, P. D.; Meunier, P. J. Effects of Long-Term Strontium Ranelate Treatment on the Risk of Nonvertebral and Vertebral Fractures in Postmenopausal Osteoporosis: Results of a Five-Year, Randomized, Placebo-Controlled Trial. *Arthritis Rheum.* **2008**, *58*, 1687−1695.
(18) Bain, S. D.; Jerome, C.; Shen, V.; Dupin-Roger, I.; Ammann, P. Strontium Ranelate Improves Bone Strength in Ovariectomized Rat by Positively Influencing Bone Resistance Determinants. *Osteoporosis Int.* **2009**, *20*, 1417−1428.
(19) Maimoun, L.; Brennan, T. C.; Badoud, I.; Dubois-Ferriere, V.; Rizzoli, R.; Ammann, P. Strontium Ranelate Improves Implant Osseointegration. *Bone* **2010**, *46*, 1436−1441.
(20) Schrooten, I.; Behets, G. J.; Cabrera, W. E.; Vercauteren, S. R.; Lamberts, L. V.; Verberckmoes, S. C.; Bervoets, A. J.; Dams, G.; Goodman, W. G.; De Broe, M. E.; D'Haese, P. C. Dose-Dependent Effects of Strontium on Bone of Chronic Renal Failure Rats. *Kidney Int.* **2003**, *63*, 927−935.
(21) Cohen-Solal, M. Strontium Overload and Toxicity: Impact on Renal Osteodystrophy. *Nephrol., Dial., Transplant.* **2002**, *17* (Suppl 2), 30−34.
(22) Andersen, O. Z.; Offermanns, V.; Sillassen, M.; Almtoft, K. P.; Andersen, I. H.; Sorensen, S.; Jeppesen, C. S.; Kraft, D. C.; Bottiger, J.; Rasse, M.; Kloss, F.; Foss, M. Accelerated Bone Ingrowth by Local Delivery of Strontium from Surface Functionalized Titanium Implants. *Biomaterials* **2013**, *34*, 5883−5890.
(23) Cheung, K. M.; Lu, W. W.; Luk, K. D.; Wong, C. T.; Chan, D.; Shen, J. X.; Qiu, G. X.; Zheng, Z. M.; Li, C. H.; Liu, S. L. Vertebroplasty by Use of a Strontium-Containing Bioactive Bone Cement. *Spine* **2005**, *30*, S84−S91.
(24) Ni, G. X.; Lu, W. W.; Chiu, K. Y.; Li, Z. Y.; Fong, D. Y.; Luk, K. D. Strontium-Containing Hydroxyapatite (Sr-Ha) Bioactive Cement for Primary Hip Replacement: An in Vivo Study. *J. Biomed. Mater. Res., Part B* **2006**, *77*, 409−415.
(25) Yu, T.; Ye, J.; Wang, Y. Preparation and Characterization of a Novel Strontium-Containing Calcium Phosphate Cement with the Two-Step Hydration Process. *Acta Biomater.* **2009**, *5*, 2717−2727.
(26) Kuang, G. M.; Yau, W. P.; Lam, W. M.; Wu, J.; Chiu, K. Y.; Lu, W. W.; Pan, H. An Effective Approach by a Chelate Reaction in Optimizing the Setting Process of Strontium-Incorporated Calcium Phosphate Bone Cement. *J. Biomed. Mater. Res., Part B* **2012**, *100*, 778−787.
(27) Schumacher, M.; Lode, A.; Helth, A.; Gelinsky, M. A Novel Strontium(Ii)-Modified Calcium Phosphate Bone Cement Stimulates Human-Bone-Marrow-Derived Mesenchymal Stem Cell Proliferation and Osteogenic Differentiation in Vitro. *Acta Biomater.* **2013**, *9*, 9547−9557.
(28) Thormann, U.; Ray, S.; Sommer, U.; Elkhassawna, T.; Rehling, T.; Hundgeburth, M.; Henss, A.; Rohnke, M.; Janek, J.; Lips, K. S.; Heiss, C.; Schlewitz, G.; Szalay, G.; Schumacher, M.; Gelinsky, M.; Schnettler, R.; Alt, V. Bone Formation Induced by Strontium Modified Calcium Phosphate Cement in Critical-Size Metaphyseal Fracture Defects in Ovariectomized Rats. *Biomaterials* **2013**, *34*, 8589−8598.
(29) Thein-Han, W. W.; Stevens, W. F. Transdermal Delivery Controlled by a Chitosan Membrane. *Drug Dev. Ind. Pharm.* **2004**, *30*, 397−404.
(30) Xu, H. H.; Weir, M. D.; Burguera, E. F.; Fraser, A. M. Injectable and Macroporous Calcium Phosphate Cement Scaffold. *Biomaterials* **2006**, *27*, 4279−4287.
(31) Kokubo, T.; Takadama, H. How Useful Is Sbf in Predicting in Vivo Bone Bioactivity? *Biomaterials* **2006**, *27*, 2907−2915.
(32) Matsubara, T.; Suardita, K.; Ishii, M.; Sugiyama, M.; Igarashi, A.; Oda, R.; Nishimura, M.; Saito, M.; Nakagawa, K.; Yamanaka, K.; Miyazaki, K.; Shimizu, M.; Bhawal, U. K.; Tsuji, K.; Nakamura, K.; Kato, Y. Alveolar Bone Marrow as a Cell Source for Regenerative Medicine: Differences between Alveolar and Iliac Bone Marrow Stromal Cells. *J. Bone Miner. Res.* **2005**, *20*, 399−409.
(33) Zou, D.; Zhang, Z.; He, J.; Zhang, K.; Ye, D.; Han, W.; Zhou, J.; Wang, Y.; Li, Q.; Liu, X.; Zhang, X.; Wang, S.; Hu, J.; Zhu, C.; Zhang, W.; zhou, Y.; Fu, H.; Huang, Y.; Jiang, X. Blood Vessel Formation in the Tissue-Engineered Bone with the Constitutively Active Form of HIF-1alpha Mediated BMSCs. *Biomaterials* **2012**, *33*, 2097−2108.
(34) Zhao, L.; Weir, M. D.; Xu, H. H. An Injectable Calcium Phosphate-Alginate Hydrogel-Umbilical Cord Mesenchymal Stem Cell Paste for Bone Tissue Engineering. *Biomaterials* **2010**, *31*, 6502−6510.
(35) Abd Samad, H.; Jaafar, M.; Othman, R.; Kawashita, M.; Abdul Razak, N. H. New Bioactive Glass-Ceramic: Synthesis and Application in Pmma Bone Cement Composites. *Biomed. Mater. Eng.* **2011**, *21*, 247−258.
(36) Ginebra, M. P.; Fernandez, E.; Boltong, M. G.; Bermudez, O.; Planell, J. A.; Driessens, F. C. Compliance of an Apatitic Calcium Phosphate Cement with the Short-Term Clinical Requirements in Bone Surgery, Orthopaedics and Dentistry. *Clin. Mater.* **1994**, *17*, 99−104.
(37) Zhang, J.; Tancret, F.; Bouler, J.-M. Fabrication and Mechanical Properties of Calcium Phosphate Cements (Cpc) for Bone Substitution. *Mater. Sci. Eng., C* **2011**, *31*, 740−747.
(38) Loty, C.; Sautier, J. M.; Boulekbache, H.; Kokubo, T.; Kim, H. M.; Forest, N. In Vitro Bone Formation on a Bone-Like Apatite Layer Prepared by a Biomimetic Process on a Bioactive Glass-Ceramic. *J. Biomed. Mater. Res.* **2000**, *49*, 423−434.
(39) Xue, W.; Moore, J. L.; Hosick, H. L.; Bose, S.; Bandyopadhyay, A.; Lu, W. W.; Cheung, K. M.; Luk, K. D. Osteoprecursor Cell Response to Strontium-Containing Hydroxyapatite Ceramics. *J. Biomed. Mater. Res., Part A* **2006**, *79*, 804−814.
(40) Valerio, P.; Pereira, M. M.; Goes, A. M.; Leite, M. F. The Effect of Ionic Products from Bioactive Glass Dissolution on Osteoblast Proliferation and Collagen Production. *Biomaterials* **2004**, *25*, 2941−2948.
(41) Silver, I. A.; Deas, J.; Erecinska, M. Interactions of Bioactive Glasses with Osteoblasts in Vitro: Effects of 45s5 Bioglass, and 58s and 77s Bioactive Glasses on Metabolism, Intracellular Ion Concentrations and Cell Viability. *Biomaterials* **2001**, *22*, 175−185.
(42) Braux, J.; Velard, F.; Guillaume, C.; Bouthors, S.; Jallot, E.; Nedelec, J.-M.; Laurent-Maquin, D.; Laquerrière, P. A New Insight into the Dissociating Effect of Strontium on Bone Resorption and Formation. *Acta Biomater.* **2011**, *7*, 2593−2603.
(43) Yang, F.; Yang, D.; Tu, J.; Zheng, Q.; Cai, L.; Wang, L. Strontium Enhances Osteogenic Differentiation of Mesenchymal Stem

DOI: 10.1021/am507008z
ACS Appl. Mater. Interfaces 2015, 7, 2393−2403

Cells and in Vivo Bone Formation by Activating Wnt/Catenin Signaling. *Stem Cells* **2011**, *29*, 981−991.
(44) Barbara, A.; Delannoy, P.; Denis, B. G.; Marie, P. J. Normal Matrix Mineralization Induced by Strontium Ranelate in Mc3t3-E1 Osteogenic Cells. *Metabolism* **2004**, *53*, 532−537.
(45) Zhang, J.; Zhao, S.; Zhu, Y.; Huang, Y.; Zhu, M.; Tao, C.; Zhang, C. Three-Dimensional Printing of Strontium-Containing Mesoporous Bioactive Glass Scaffolds for Bone Regeneration. *Acta Biomater.* **2014**, *10*, 2269−2281.
(46) Lin, K.; Xia, L.; Li, H.; Jiang, X.; Pan, H.; Xu, Y.; Lu, W. W.; Zhang, Z.; Chang, J. Enhanced Osteoporotic Bone Regeneration by Strontium-Substituted Calcium Silicate Bioactive Ceramics. *Biomaterials* **2013**, *34*, 10028−10042.
(47) Xynos, I. D.; Edgar, A. J.; Buttery, L. D.; Hench, L. L.; Polak, J. M. Gene-Expression Profiling of Human Osteoblasts Following Treatment with the Ionic Products of Bioglass 45s5 Dissolution. *J. Biomed. Mater. Res.* **2001**, *55*, 151−157.
(48) Bonnelye, E.; Chabadel, A.; Saltel, F.; Jurdic, P. Dual Effect of Strontium Ranelate: Stimulation of Osteoblast Differentiation and Inhibition of Osteoclast Formation and Resorption in Vitro. *Bone* **2008**, *42*, 129−138.
(49) Chattopadhyay, N.; Quinn, S. J.; Kifor, O.; Ye, C.; Brown, E. M. The Calcium-Sensing Receptor (Car) Is Involved in Strontium Ranelate-Induced Osteoblast Proliferation. *Biochem. Pharmacol.* **2007**, *74*, 438−447.
(50) Hurtel-Lemaire, A. S.; Mentaverri, R.; Caudrillier, A.; Cournarie, F.; Wattel, A.; Kamel, S.; Terwilliger, E. F.; Brown, E. M.; Brazier, M. The Calcium-Sensing Receptor Is Involved in Strontium Ranelate-Induced Osteoclast Apoptosis New Insights into the Associated Signaling Pathways. *J. Biol. Chem.* **2009**, *284*, 575−584.
(51) Caverzasio, J. Strontium Ranelate Promotes Osteoblastic Cell Replication through at Least Two Different Mechanisms. *Bone* **2008**, *42*, 1131−1136.
(52) Li, Y.; Li, Q.; Zhu, S.; Luo, E.; Li, J.; Feng, G.; Liao, Y.; Hu, J. The Effect of Strontium-Substituted Hydroxyapatite Coating on Implant Fixation in Ovariectomized Rats. *Biomaterials* **2010**, *31*, 9006−9014.
(53) Vestermark, M. T.; Hauge, E. M.; Soballe, K.; Bechtold, J. E.; Jakobsen, T.; Baas, J. Strontium Doping of Bone Graft Extender. *Acta Orthop.* **2011**, *82*, 614−621.
(54) Bauer, T. W.; Schils, J. The Pathology of Total Joint Arthroplasty.Ii. Mechanisms of Implant Failure. *Skeletal Radiol.* **1999**, *28*, 483−497.
(55) Peng, S.; Liu, X. S.; Wang, T.; Li, Z.; Zhou, G.; Luk, K. D.; Guo, X. E.; Lu, W. W. In Vivo Anabolic Effect of Strontium on Trabecular Bone Was Associated with Increased Osteoblastogenesis of Bone Marrow Stromal Cells. *J. Orthop. Res.* **2010**, *28*, 1208−1214.

DOI: 10.1021/am507008z
ACS Appl. Mater. Interfaces 2015, 7, 2393−2403